catalysts

MDPI

Article

Metallic–Organic Cages (MOCs) with Heterometallic Character: Flexibility-Enhancing MOFs

Sergio Posada-Pérez [1], Jordi Poater [2,3,*], Naeimeh Bahri-Laleh [4] and Albert Poater [1,*]

[1] Institut de Química Computacional i Catàlisi, Departament de Química, Universitat de Girona, c/Mª Aurèlia Capmany, 17003 Girona, Spain
[2] Departament de Química Inorgànica i Orgànica & IQTCUB, Universitat de Barcelona, 08028 Barcelona, Spain
[3] ICREA, 08010 Barcelona, Spain
[4] Polymerization Engineering Department, Iran Polymer and Petrochemical Institute (IPPI), Tehran P.O. Box 14965/115, Iran
* Correspondence: jordi.poater@ub.edu (J.P.); albert.poater@udg.edu (A.P.); Tel.: +34-(972)-419403 (A.P.)

Abstract: The dichotomy between metal–organic frameworks (MOFs) and metal–organic cages (MOCs) opens up the research spectrum of two fields which, despite having similarities, both have their advantages and disadvantages. Due to the fact that they have cavities inside, they also have applicability in the porosity sector. Bloch and coworkers within this evolution from MOFs to MOCs manage to describe a MOC with a structure of Cu_2 paddlewheel Cu_4L_4 (L = bis(pyrazolyl)methane) with high precision thanks to crystallographic analyses of X-ray diffraction and also SEM-EDX. Then, also at the same level of concreteness, they were able to find the self-assembly of $Pd(II)Cl_2$ moieties on the available nitrogen donor atoms leading to a $[Cu_4(L(PdCl_2))_4]$ structure. Here, calculations of the DFT density functional allow us to reach an unusual precision given the magnitude and structural complexity, explaining how a pyrazole ring of each bis(pyprazolyl)methane ligand must rotate from an *anti* to a *syn* conformation, and a truncation of the MOC structure allows us to elucidate, in the absence of the MOC constraint and its packing in the crystal, that the rotation is almost barrierless, as well as also explain the relative stability of the different conformations, with the *anti* being the most stable conformation. Characterization calculations with Mayer bond orders (MBO) and noncovalent interaction (NCI) plots discern what is important in the interaction of this type of cage with $PdCl_2$ moieties, also $CuCl_2$ by analogy, as well as simple molecules of water, since the complex is stable in this solvent. However, the L ligand is proved to not have the ability to stabilize an H_2O molecule.

Keywords: COF; MOF; metallic–organic cage; pyrazole; bis(pyrazolyl)methane; heterometallic

check for updates

Citation: Posada-Pérez, S.; Poater, J.; Bahri-Laleh, N.; Poater, A. Metallic–Organic Cages (MOCs) with Heterometallic Character: Flexibility-Enhancing MOFs. *Catalysts* **2023**, *13*, 317. https://doi.org/10.3390/catal13020317

Academic Editors: Somboon Chaemchuen and Francis Verpoort

Received: 31 December 2022
Revised: 19 January 2023
Accepted: 26 January 2023
Published: 1 February 2023

Copyright: © 2023 by the authors. Licensee MDPI, Basel, Switzerland. This article is an open access article distributed under the terms and conditions of the Creative Commons Attribution (CC BY) license (https://creativecommons.org/licenses/by/4.0/).

1. Introduction

The evolution of the petrochemical industry during the 19th century, combined with the fact that the oil industry began to exploit the goodness of catalysis in processes such as the catalytic (hydro)cracking in the 1929s [1,2], led to the explosion of the polymer research field. Consequently, a new bunch of materials, including acrylonitrile and vinyl chlorides [3,4], and then followed by polymeric films and synthetic fibers including cellophane, nylon, rayon and polyester [5,6], have become essential in our everyday life. Despite the multiple advantages of polymers, there was a demand for new materials capable of enjoying macromolecular properties, such as polymers with more order and a clear structure, but at the same time also with storage capacity and even catalytic activity. This role could then be played by metal–organic frameworks (MOFs) [7,8], but with a fairly common drawback which is the lack of flexibility [9,10]. Since the 2000s, the simple change of infinite units of the frameworks could be changed to units with the metal–organic cages (MOC)s. They can also be called nanocapsules if they are meant to be a simple selective wrapper [11]. MOCs, among other properties, some still to be explored, present in the solid state the ability to modulate porosity [12,13], and in both the solid state and in the liquid state, to interact

perfectly in highly selective host–guest systems [14–16]. These properties are not sterile, since they derive a wide range of applications from being reactive in simple systems, transporters [17–19], storage [20,21] or gas separators [22–24], or even being proactive in the field of sensors [25,26] or catalysis [27–29]. MOCs have also guided materials science towards new materials [30,31] and composites [32], from quasi-two-dimensional membranes [33,34] to three-dimensional networks or gels [35–39].

The MOCs synthesized so far, not by will but for simplicity, are composed of a single metal [40], and are designated as homometallic. To increase the scope of applications [41,42], once the range of ligands has been updated and expanded [43–47], two major strategies of work have been opened in MOCs that can be combined: increasing the complexity of the ligands [48,49] and/or adding different metal units to the original, that is, evolving to heterometallic MOCs [50,51], in analogy with bimetallic MOFs [52]. Despite the advantages of heterometallic MOCs, they still suffer from being materials that are practically only used for basic research since their synthesis is not trivial [53], and only small amounts are producible, often leading to homometallic MOCs, but this is being remedied by a battery of new solutions based on the assembly of already consolidated units [54–61], with special emphasis on the electron-donating capacity of the agents [62,63].

Since 2020, a series of works with paddlewheel-derived M_nL_n MOCs with M(II), including copper, rhodium and chromium [64–66], have led to multifunctional materials. More interestingly, the addition of N-donor ligands allowed the assembly of MOCs thanks to axial coordination sites on the surface of the cage [67–69]. Particularly, Bloch et al. have been able to combine Cu_4L_4 MOCs with bis(pyrazolyl)methane sites. The MOC resulting from the synthesis in Scheme 1 led to a subsequent assembly of simple metal halides [70,71].

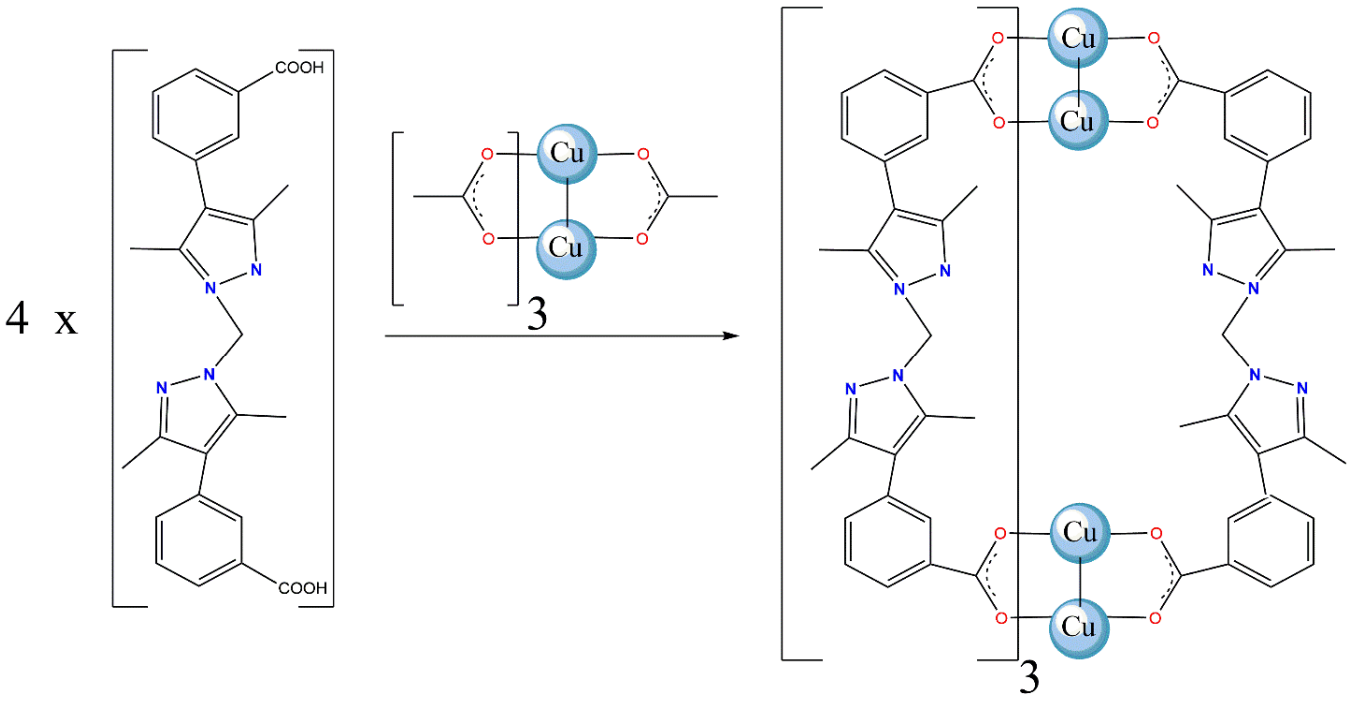

Scheme 1. Schematic synthesis of the ***anti*-MOC**, resulting from the combination of b(3-cp-bdmpm) ligand (L) and $Cu_2(OAc)_4$ in DMF.

Then, Bloch and coworkers obtained a crystallographic series that confirms the flexibility of the bis(pyrazolyl)methane site [70], observing MOC conformations as being either *syn* or *anti*, regardless. However, when the heterometallic system is obtained, the conformation is only in *syn*. Interestingly, the same research group previously achieved MOFs with the same organic ligand with the consequent increase in rigidity and low porosity [72–75]. Nevertheless, the post metalation of MOFs is relatively facile, while the same process on MOCs

is a challenge synthetically speaking [76]. In view of the flexible character of the pyrazoles of Cu(II)-Pd(II) heterooctametallic cage-type complexes [77], and with the applicability as porous agents, density functional theory (DFT) calculations were performed with the aim of rationalizing the reversibility of the above structures.

2. Results

The calculations started from the crystallographic structure of the ***anti*-MOC** included in Scheme 1, checking what it means to have the axial positions of the copper atoms saturated with dimethylformamide (DMF) molecules, replaced by simple formaldehydes. However, the stabilizing effect, despite its multiplicative power, for each of the eight copper atoms in the cage, is compensated by the entropic cost, thus leaving a destabilization, but only of 2.5 kcal/mol. Thus, it is intriguing to understand the structural features of the current MOC, considering the rules of maximum site occupancy [78,79].

The Mayer bond orders (MBOs) [80] were calculated using the equation based on the atomic orbital overlap matrix and the α and β electron density matrices. It is a method to describe the interaction between two fragments, and by default also the strength of any bond [81]. Actually, the MBOs are fundamental here to screen how strong the Cu_2 linkers are, in particular the Cu-Cu bond [82], with a remarkable value of 0.426 with formaldehydes on each copper center, while nearly constantly removing the latter molecules, with a MBO of 0.412. This allows us to remark that the formaldehyde coordination is rather weak with a MBO of 0.178 [10,83].

The most important thing about binding solvent molecules to copper atoms is that it involves the saturation of the inside of the cage. Then, to study the bis(pyrazolyl)methane site, the crystallographic *anti* conformation ***anti*-MOC** (Scheme 2a), owing the four existing bis(pyrazolyl)methane sites of the cage in *anti* fashion, was taken into account, and the conversion to *syn* thermodynamically entailed a destabilization of 2.5, 3.2, 4.1 and 4.7 kcal/mol, respectively, transforming from one to four sites, leading finally to ***syn*-MOC** (Scheme 2b). It should be mentioned that the movement of the pyrazole ring forming the syn conformation was tackled so that the four different centers were arranged symmetrically, that is, with a pseudo symmetry of c4v between them, or a c2v typology. It should be mentioned that the second was less stable by 3.3 kcal/mol. The effect is robust, because by converting three of the four groups into *syn* instead of completeness, the less symmetrical conformation was also unfavored, but by only 0.8 kcal/mol. However, the initial anti structure always remains as the most stable, by at least 1.3 kcal/mol. Therefore, the small differences are almost unappreciable, and the motion dynamics of the cage will lead to one or the other indiscriminately, which explains that crystallographically when the cage uses bis(pyrazolyl)methane moiety as a bidentate ligand both the pseudo c2v conformations are formed like c4v [70].

To study thermodynamically and above all kinetically how the transition from *anti* to *syn* with respect to the two pyrazole groups of the bis(pyrazolyl)methane moiety occurs, the system was truncated (see Figure 1), simply taking the organic bis(pyrazolyl)methane moiety. Thus, the *anti*-bis(pyrazolyl)methane (***anti*-O**) structure was brought to the *syn* conformation, reaching the isomer of ***syn*-O**, 0.5 kcal/mol less stable. Structurally, the N-C-N-N dihedral angle evolves from 85.1° to −121.7°. Due to the interconversion between conformations the reaction path must go through **TS1**, i.e., a transition state located 2.2 kcal/mol above ***anti*-O**, with a dihedral angle of −103.7°, in perfect agreement with similar rotations [84]. If the pyrazole ring would rotate in the reverse direction, there is more steric hindrance due to the methyl located alpha to the nitrogen atom, but simply this **TS2** requires an additional kinetic cost of 2.4 kcal/mol and the dihedral angle is −168.4° instead of 1.5° for **TS1**. In addition, the movement of the rotation of one of the pyrazole rings is of a small dimension that, in the conformation of the MOC, would also be feasible with all certainty, although a little more constrained. It is of such a small dimension that quantum mechanics makes its calculation difficult, and this is evident with an imaginary frequency of 17.0 and 24.2 cm^{-1} for **TS1** and **TS2**, respectively, but only **TS1** would be

feasible since the rotation in the case of the **TS2** would be prevented by the cage itself. On the other hand, ***syn*-O** fails to have c2v symmetry, and in fact, instead of being an intermediate, it is a transition state, which requires only a barrier of 2.0 kcal/mol, with a dihedral angle of −80.9°. It actually corresponds to the transition state that binds the two enantiomers of the *syn* conformation.

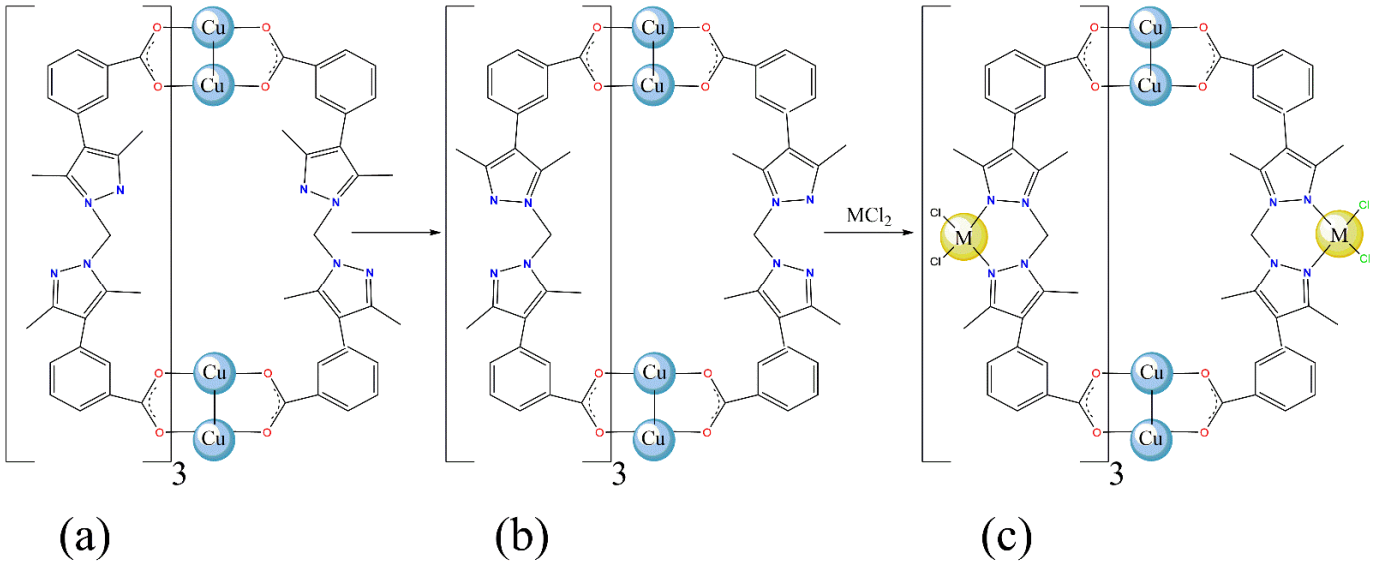

Scheme 2. Schematic Lewis structures of (**a**) ***anti*-MOC**; (**b**) ***syn*-MOC**; and (**c**) ***syn*-MOC-MCl_2** (M = Pd or Cu; the four ligands around each copper atom in the linker are placed in a squared planar geometry).

To understand how the bis(pyrazolyl)methane sites are orientated, we computed the noncovalent interactions (NCI) plots using the NCIPLOT package of Contreras-García and coworkers [85,86]. NCI diagrams allow a qualitative analytical study of the strength of noncovalent interactions between different fragments. Since in Figure 2a the interaction among sites is null, missing interactions between aromatic rings [87], we centered our analysis on the truncated structures. Knowing the low covalent character presented by the interaction between all the N atoms of the pyrazolyl moieties, the hydrogen atoms of the methylene bridge, or methyl substituents, the NCI plots in Figure 2 not only qualitatively evaluate the strength of the noncovalent interactions, but they are able to conclude the preference for the *anti* conformation of the bis(pyrazolyl)methane sites, since more favorable interactions are included when the nitrogen atoms of both pyrazole rings are placed farther from each other [10]. This is thanks to N···H interactions, corresponding to the closest H atom of the methyl group, while for the *syn* conformation these interactions do not exist. The current study, where a single cage misses the observed intermolecular hydrogen bonding between the two methylene bridge hydrogens and the nitrogen atoms of the adjacent cage molecules that were observed in the extended crystal packing, with expected H-bonds of around 2.4 Å, is thus of remarkable importance compared to the homologous intramolecular H-bonds which are placed at slightly less than 2.6 Å.

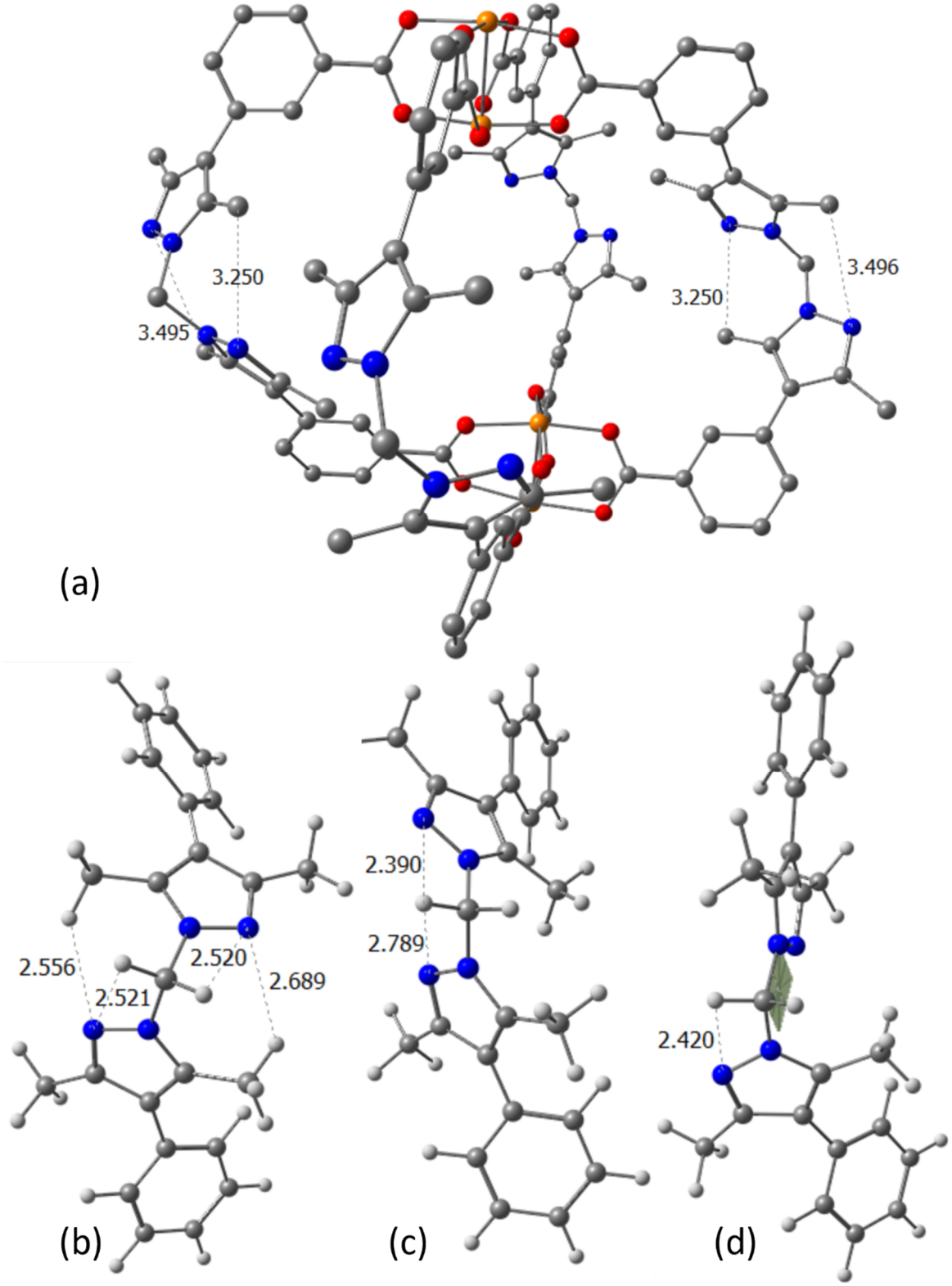

Figure 1. (**a**) Optimized structure of the ***anti*-MOC** (H atoms are removed for the sake of clarity): the truncated (**b**) ***anti*-O** and (**c**) ***syn*-O** bis(pyrazolyl)methane sites and (**d**) **TS1** corresponding to the isomerization of the *anti* to the *syn* conformation with a dihedral angle of −103.7° (selected distances in Å, see Table S1 in the Supplementary Information for further details).

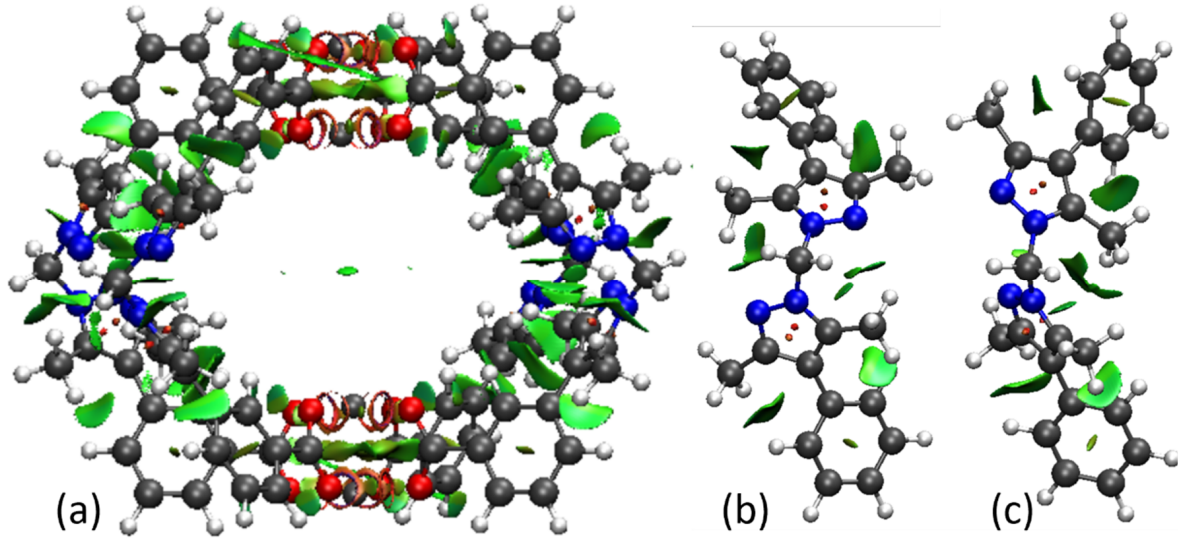

Figure 2. NCI plots of (**a**) MOC and the truncated (**b**) ***anti*-O** and (**c**) ***syn*-O** bis(pyrazolyl)methane sites. The isosurface represents a value of 0.5 with a color scale for the reduced density gradient (green is attractive while red is repulsive).

Since paddlewheels are often related to water [88,89], and to address the importance of the crystal of the MOC with a water molecule achieved by Bloch and coworkers [70], DFT calculations unveiled the nonexistence of a strong interaction with a water molecule, and such a structure could be defined simply as an adduct, with a remarkable H-bond placed at 1.891 Å. From the thermodynamic point of view, the coordination of a water molecule was found to be unfavorable by 5.6 and 7.5 kcal/mol, respectively, owing or not to axial ligands on the copper acetate centers, respectively, and for the truncated ***anti*-O** again unfavored by 5.6 kcal/mol. Thus, this leads to the conclusion that the packing of the crystal helped to sequester a water molecule close to two pyrazolic N-donor atoms from two cages.

Following the experimental crystallographic effort of Bloch and coworkers [70], where they were able to complexate $PdCl_2$ moieties on the ***syn*-MOC** and then obtain crystals of the combination, the truncated ***syn*-MOC** structure with metal centers in all four sites was consequently optimized. In particular, the $PdCl_2$ unit was chosen for the simplicity (see Scheme 2c) and also then for the comparative effect of the copper counterpart. Formulating the direct equation for the formation of the heterometallic complex is highly complex since it is made from the monomer $PdCl_2$ (or $CuCl_2$ in the case of copper, which would obviously not be heterometallic, but the two metal centers are of different natures anyway). However, it is a thermodynamically favored process by almost 50 kcal/mol, and it should be mentioned that for palladium this process is 23.2 kcal/mol more stable than for copper. Going further by analyzing the energy decomposition, the fragment that undergoes the most deformational change is the organic one with 4.6 kcal/mol (5.1 kcal/mol for copper), while the metallic part undergoes negligible deformation of 0.9 kcal/mol. In fact, it explains that to force a structure of an organic ligand almost with c2v symmetry, as it was explained above, implies a destabilization, but this was then widely surpassed by the formation of the squared planar center around the metal. Structurally, to validate more consistently the comparison between metals [90], the results of MBOs for the metal-N bonds reinforce the stronger character of the Pd-N bonds (0.486) compared to the Cu-N bonds (0.441) [91,92].

3. Computational Details

Density functional theory (DFT) calculations were performed with the Gaussian16 package [93]. Without symmetry constraints, the geometry optimizations were carried out via the spin-restricted Kohn–Sham (RKS) formalism and employing the M06L GGA functional of Zhao and Truhlar [94]. The double-zeta polarization basis set Def2-SVP keyword was

used for all atoms [95,96]. Frequency calculations were carried out to confirm the nature of the stationary points. The reported Gibbs energies in the current work contain electronic energies obtained at the M06L/Def2-TZVP level of theory corrected with zero-point energies, thermal corrections and entropy effects evaluated at 298.15 K, achieved at the M06L/Def2SVP level plus a solvation contribution evaluated by the SMD continuum solvation model, a variation of the IEFPCM of Truhlar and co-workers [97], based on the quantum mechanical charge density of the solute interacting with a continuum description of the solvent (dimethylformamide).

4. Conclusions

MOCs represent a very promising class of metal-organic materials (MOFs) in terms of host-host binding ability related to their well-defined cavities and engineered pores. Discrete MOCs can also be thought of as infinite cage-based frameworks that use each MOC unit as supramolecular building blocks. And among the advantages, we have the relative solubility and stability of MOCs. Despite the complexity of the MOC structure, containing hundreds of atoms, DFT calculations, without losing the robustness of the results, have allowed us to understand the flexibility of a recently synthesized structure of Cu_4L_4 MOC, functionalized with non-coordinating bis(pyrazolyl)methane sites. The heterometallic character was achieved with the inclusion of palladium metal halides (and also by comparison with copper), demonstrating that thermodynamics favor the process, and the kinetics of rotation of a pyrazole to have *syn* conformations of the two N-donor atoms in each bis(pyrazolyl)methane center is entirely feasible. On the other hand, it is confirmed that the interaction of a molecule outside the cage is not of strong nature and is due to a simple misfortune of the packing of the crystals. The porosity of the systems paves the way for ongoing calculations to understand if the porosity of the system allows molecules to be stabilized, not outside the cage [98], but inside it and selectively [23].

In the discussion of the results above, the truncation of the bis(pyrazolyl)methane site allows us to understand how one of the pyrazole rings rotates, but it must be understood that the cage imposes a constraint that undoubtedly makes movement a little difficult, and in an MOF it might reach the point of not being possible. Indeed, this is an experimental example where the calculations find the reason for the need to have a cage, and not in a framework format. It is a decisive step towards the achievement of new structures [99] and not a step back from MOFs, but it paves the way to widening the applicability of the structures that have already been generated in the field of MOFs. In short, this study has allowed us to understand that the flexibility of pyrazoles is the driving force of the selectivity of the coordinating capacity in metal assembly.

Supplementary Materials: The following supporting information can be downloaded at: https://www.mdpi.com/article/10.3390/catal13020317/s1, Table S1: xyz coordinates and absolute energies (in a.u.) of all computed DFT species.

Author Contributions: Experiments, data curation, analysis of data: S.P.-P., N.B.-L., J.P. and A.P.; conceptualization, A.P.; writing—review and editing, S.P.-P., J.P., A.P. and N.B.-L. All authors have read and agreed to the published version of the manuscript.

Funding: This research was funded by Ministerio de Ciencia e Innovación for the project PID2021-127423NB-I00; the Generalitat de Catalunya (project 2021 SGR0623 and ICREA Academia prize 2019 to A.P.). N.B.-L. appreciates the support of the Iran National Science Foundation (INSF) for the grant number 4006310. S.P.-P. appreciates the economic support of Marie Curie fellowship (H2020-MSCA-IF-2020-101020330). J.P. acknowledges the Spanish Ministerio de Ciencia e Innovación (PID2019-106830GB-I00, CEX2021-001202-M and MDM-2017-0767).

Data Availability Statement: Data is contained within the article or supplementary material.

Acknowledgments: A.P. is a Serra Húnter Fellow and thanks the ICREA Academia prize 2019. S.P.-P. thanks the Marie Curie fellowship.

Conflicts of Interest: The authors declare no conflict of interest.

References

1. American Chemical Society National Historic Chemical Landmarks. The Houdry Process for Catalytic Cracking. Available online: http://www.acs.org/content/acs/en/education/whatischemistry/landmaks/houdry.html (accessed on 24 December 2022).
2. Spitz, P.H. *Petrochemicals: The Rise of an Industry*; John Wiley and Sons, Inc.: New York, NY, USA, 1988; pp. 184–191.
3. Weirsselmel, K.; Arpe, H.J. *Industrial Organic Chemistry*, 3rd ed.; VCH Publishers, Inc.: New York, NY, USA, 1997; p. 218.
4. Worthy, W. Canadian chemical firms: Another good year. *Chem. Eng. News* **1979**, *57*, 17. [CrossRef]
5. History. Available online: http://www.dupont.com/corporate-functions/our-company/dupont-history.html (accessed on 24 December 2022).
6. Schröder, G. *Ullmann's Encyclopedia of Industrial Chemistry*; John Wiley and Sons, Inc.: Hoboken, NJ, USA, 2012; Volume 28, pp. 481–485.
7. Hilal, M.E.; Aboulouard, A.; Akbar, A.R.; Younus, H.A.; Horzum, N.; Verpoort, F. Progress of MOF-derived functional materials toward industrialization in solar cells and metal-air batteries. *Catalysts* **2020**, *10*, 897. [CrossRef]
8. Hosono, N.; Kitagawa, S. Modular Design of Porous Soft Materials via Self-Organization of Metal—Organic Cages. *Acc. Chem. Res.* **2018**, *51*, 2437–2446. [CrossRef] [PubMed]
9. Pareras, G.; Detiana, D.; Poater, A. MOF encapsulation of Ru olefin metathesis catalysts to block catalyst decomposition. *Catalysts* **2020**, *10*, 687. [CrossRef]
10. Poater, J.; Gimferrer, M.; Poater, A. Covalent and Ionic Capacity of MOFs To Sorb Small Gas Molecules. *Inorg. Chem.* **2018**, *57*, 6981–6990. [CrossRef]
11. Colomban, C.; Szalóki, G.; Allain, M.; Gómez, L.; Goeb, S. Reversible C60 Ejection from a Metallocage through the Redox-Dependent Binding of a Competitive Guest. *Chem. Eur. J.* **2018**, *23*, 3016–3022. [CrossRef]
12. Sánchez-González, E.; Tsang, M.Y.; Troyano, J.; Craig, G.A.; Furukawa, S. Assembling Metal—Organic Cages as Porous Mate-rials. *Chem. Soc. Rev.* **2022**, *51*, 4876–4889. [CrossRef]
13. Gosselin, E.J.; Rowland, C.A.; Bloch, E.D. Permanently Microporous Metal—Organic Polyhedra. *Chem. Rev.* **2020**, *120*, 8987–9014. [CrossRef]
14. Rizzuto, F.J.; von Krbek, L.K.S.; Nitschke, J.R. Strategies for Binding Multiple Guests in Metal—Organic Cages. *Nat. Rev. Chem.* **2019**, *3*, 204–222. [CrossRef]
15. Cook, T.R.; Stang, P.J. Recent Developments in the Preparation and Chemistry of Metallacycles and Metallacages via Coor-dination. *Chem. Rev.* **2015**, *115*, 7001–7045. [CrossRef]
16. Dalgarno, S.J.; Power, N.P.; Atwood, J.L. Metallo-Supramolecular Capsules. *Coord. Chem. Rev.* **2008**, *252*, 825–841. [CrossRef]
17. Zhu, W.; Guo, J.; Ju, Y.; Serda, R.E.; Croissant, J.G.; Shang, J.; Coker, E.; Agola, J.O.; Zhong, Q.-Z.; Ping, Y.; et al. Modular Metal—Organic Polyhedra Superassembly: From Molecular-Level Design to Targeted Drug Delivery. *Adv. Mater.* **2019**, *31*, 1806774. [CrossRef] [PubMed]
18. Zava, O.; Mattsson, J.; Therrien, B.; Dyson, P.J. Evidence for Drug Release from a Metalla-Cage Delivery Vector Following Cellular Internalisation. *Chem. Eur. J.* **2010**, *16*, 1428–1431. [CrossRef] [PubMed]
19. Lewis, J.E.M.; Gavey, E.L.; Cameron, S.A.; Crowley, J.D. Stimuli-Responsive Pd2L4 Metallosupramolecular Cages: Towards Targeted Cisplatin Drug Delivery. *Chem. Sci.* **2012**, *3*, 778–784. [CrossRef]
20. Deegan, M.M.; Dworzak, M.R.; Gosselin, A.J.; Korman, K.J.; Bloch, E.D. Gas Storage in Porous Molecular Materials. *Chem. Eur. J.* **2021**, *27*, 4531–4547. [CrossRef]
21. Duriska, M.B.; Neville, S.M.; Lu, J.; Iremonger, S.S.; Boas, J.F.; Kepert, C.J.; Batten, S.R. Systematic Metal Variation and Solvent and Hydrogen-Gas Storage in Supramolecular Nanoballs. *Angew. Chem. Int. Ed.* **2009**, *48*, 8919–8922. [CrossRef]
22. Lorzing, G.R.; Trump, B.A.; Brown, C.M.; Bloch, E.D. Selective Gas Adsorption in Highly Porous Chromium(II)-Based Metal—Organic Polyhedra. *Chem. Mater.* **2017**, *29*, 8583–8587. [CrossRef]
23. Fan, W.; Peh, S.B.; Zhang, Z.; Yuan, H.; Yang, Z.; Wang, Y.; Chai, K.; Sun, D.; Zhao, D. Tetrazole-Functionalized Zirconium Metal-Organic Cages for Efficient C_2H_2/C_2H_4 and C_2H_2/CO_2 Separations. *Angew. Chem. Int. Ed.* **2021**, *60*, 17338–17343. [CrossRef]
24. Zhu, J.-L.; Zhang, D.; Ronson, T.K.; Wang, W.; Xu, L.; Yang, H.-B.; Nitschke, J.R. A Cavity-Tailored Metal-Organic Cage Entraps Gases Selectively in Solution and the Amorphous Solid State. *Angew. Chem. Int. Ed.* **2021**, *60*, 11789–11792. [CrossRef]
25. Yan, X.; Cook, T.R.; Wang, P.; Huang, F.; Stang, P.J. Highly Emissive Platinum(II) Metallacages. *Nat. Chem.* **2015**, *7*, 342–348. [CrossRef]
26. Brzechwa-Chodzyńska, A.; Drożdż, W.; Harrowfield, J.; Stefankiewicz, A.R. Fluorescent Sensors: A Bright Future for Cages. *Coord. Chem. Rev.* **2021**, *434*, 213820. [CrossRef]
27. Martí-Centelles, V.; Lawrence, A.L.; Lusby, P.J. High Activity and Efficient Turnover by a Simple, Self-Assembled "Artificial Diels—Alderase". *J. Am. Chem. Soc.* **2018**, *140*, 2862–2868. [CrossRef] [PubMed]
28. Brown, C.J.; Toste, F.D.; Bergman, R.G.; Raymond, K.N. Supramolecular Catalysis in Metal—Ligand Cluster Hosts. *Chem. Rev.* **2015**, *115*, 3012–3035. [CrossRef] [PubMed]
29. Xue, Y.; Hang, X.; Ding, J.; Li, B.; Zhu, R.; Pang, H.; Xu, Q. Catalysis within Coordination Cages. *Coord. Chem. Rev.* **2021**, *430*, 213656. [CrossRef]
30. Gosselin, A.J.; Antonio, A.M.; Korman, K.J.; Deegan, M.M.; Yap, G.P.A.; Bloch, E.D. Elaboration of Porous Salts. *J. Am. Chem. Soc.* **2021**, *143*, 14956–14961. [CrossRef] [PubMed]

31. Antonio, A.M.; Korman, K.J.; Yap, G.P.A.; Bloch, E.D. Porous Metal−Organic Alloys Based on Soluble Coordination Cages. *Chem. Sci.* **2020**, *11*, 12540–12546. [CrossRef]
32. Li, T.-T.; Liu, S.-N.; Wu, L.-H.; Cai, S.-L.; Zheng, S.-R. Strategies for the Construction of Functional Materials Utilizing Presynthesized Metal-Organic Cages (MOCs). *ChemPlusChem* **2022**, *87*, e202200172. [CrossRef]
33. Zhu, G.; O'Nolan, D.; Lively, R.P. Molecularly Mixed Composite Membranes: Challenges and Opportunities. *Chem. Eur. J.* **2020**, *26*, 3464–3473. [CrossRef]
34. Yang, Z.; Liu, G.; Yuan, Y.D.; Peh, S.B.; Ying, Y.; Fan, W.; Yu, X.; Yang, H.; Wu, Z.; Zhao, D. Homoporous Hybrid Membranes Containing Metal-Organic Cages for Gas Separation. *J. Memb. Sci.* **2021**, *636*, 119564. [CrossRef]
35. Legrand, A.; Liu, L.-H.; Royla, P.; Aoyama, T.; Craig, G.A.; Carné-Sánchez, A.; Urayama, K.; Weigand, J.J.; Lin, C.-H.; Fu-rukawa, S. Spatiotemporal Control of Supramolecular Polymerization and Gelation of Metal—Organic Polyhedra. *J. Am. Chem. Soc.* **2021**, *143*, 3562–3570. [CrossRef]
36. Oldenhuis, N.J.; Qin, K.P.; Wang, S.; Ye, H.-Z.; Alt, E.A.; Willard, A.P.; Van Voorhis, T.; Craig, S.L.; Johnson, J.A. Pho-toswitchable Sol—Gel Transitions and Catalysis Mediated by Polymer Networks with Coumarin-Decorated $Cu_{24}L_{24}$ Met-al—Organic Cages as Junctions. *Angew. Chem. Int. Ed.* **2020**, *59*, 2784–2792. [CrossRef] [PubMed]
37. Grancha, T.; Carné-Sánchez, A.; Zarekarizi, F.; Hernández-López, L.; Albalad, J.; Khobotov, A.; Guillerm, V.; Morsali, A.; Juanhuix, J.; Gándara, F.; et al. Synthesis of Polycarboxylate Rhodium(II) Metal—Organic Polyhedra (MOPs) and Their Use as Building Blocks for Highly Connected Metal−Organic Frameworks (MOFs). *Angew. Chem. Int. Ed.* **2021**, *60*, 5729–5733. [CrossRef] [PubMed]
38. Pan, Y.; Rao, C.; Tan, X.; Ling, Y.; Singh, A.; Kumar, A.; Li, B.; Liu, J. Cobalt-seamed C-methylpyrogallol[4]arene nanocapsules-derived magnetic carbon cubes as advanced adsorbent toward drug contaminant removal. *Chem. Eng. J.* **2022**, *433*, 133857. [CrossRef]
39. Rao, C.; Zhou, L.; Pan, Y.; Lu, C.; Qin, X.; Sakiyama, H.; Muddassir, M.; Liu, J. The extra-large calixarene-based MOFs-derived hierarchical composites for photocatalysis of dye: Facile syntheses and contribution of carbon species. *J. Alloys Compd.* **2022**, *897*, 163178. [CrossRef]
40. Lee, S.; Jeong, H.; Nam, D.; Lah, M.S.; Choe, W. The Rise of Metal—Organic Polyhedra. *Chem. Soc. Rev.* **2021**, *50*, 528–555. [CrossRef]
41. Hardy, M.; Tessarolo, J.; Holstein, J.J.; Struch, N.; Wagner, N.; Weisbarth, R.; Engeser, M.; Beck, J.; Horiuchi, S.; Clever, G.H.; et al. A Family of Heterobimetallic Cubes Shows Spin-Crossover Behaviour Near Room Temperature. *Angew. Chem. Int. Ed.* **2021**, *60*, 22562–22569. [CrossRef]
42. Hu, X.; Han, M.; Shao, L.; Zhang, C.; Zhang, L.; Kelley, S.P.; Zhang, C.; Lin, J.; Dalgarno, S.J.; Atwood, D.A.; et al. Self-Assembly of a Semiconductive and Photoactive Heterobimetallic Metal—Organic Capsule. *Angew. Chem. Int. Ed.* **2021**, *60*, 10516–10520. [CrossRef]
43. Bloch, W.M.; Clever, G.H. Integrative Self-Sorting of Coordination Cages Based on "naked" Metal Ions. *Chem. Commun.* **2017**, *53*, 8506–8516. [CrossRef]
44. Bloch, W.M.; Holstein, J.J.; Hiller, W.; Clever, G.H. A "Doubly-Bridged Figure-Eight:" Morphological Control of Heteroleptic Cis- and Trans-$Pd_2L_2L'_2$ Cages. *Angew. Chem. Int. Ed.* **2017**, *56*, 8285–8289. [CrossRef]
45. Walker, S.E.; Boer, S.A.; Malcomson, T.; Paterson, M.J.; Tuck, K.L.; Turner, D.R. Steric Control of Sorting Regimes in Self-Assembled Cages. *Chem. Commun.* **2021**, *57*, 12456–12459. [CrossRef]
46. Preston, D.; Barnsley, J.E.; Gordon, K.C.; Crowley, J.D. Controlled Formation of Heteroleptic $[Pd_2(L_a)_2(L_b)_2]^{4+}$ Cages. *J. Am. Chem. Soc.* **2016**, *138*, 10578–10585. [CrossRef] [PubMed]
47. Li, J.R.; Zhou, H.C. Bridging-Ligand-Substitution Strategy for the Preparation of Metal-Organic Polyhedra. *Nat. Chem.* **2010**, *2*, 893–898. [CrossRef] [PubMed]
48. Markwell-Heys, A.W.; Schneider, M.L.; Marie, J.; Madridejos, L.; Metha, G.F.; Bloch, W.M. Self-Sorting of Porous $Cu_4L_2L'_2$ Metal-Organic Cages Composed of Isomerisable Ligands. *Chem. Commun.* **2021**, *57*, 2915–2918. [CrossRef] [PubMed]
49. Lewis, J.E.M.; Crowley, J.D. Metallo-Supramolecular Self-Assembly with Reduced-Symmetry Ligands. *ChemPlusChem* **2020**, *85*, 815–827. [CrossRef]
50. Hardy, M.; Lützen, A. Better Together: Functional Heterobimetallic Macrocyclic and Cage-like Assemblies. *Chem. Eur. J.* **2020**, *26*, 13332–13346. [CrossRef]
51. Li, H.; Yao, Z.-J.; Liu, D.; Jin, G.-X. Multi-Component Coordination-Driven Self-Assembly toward Heterometallic Macrocycles and Cages. Coord. *Chem. Rev.* **2015**, *293–294*, 139–157.
52. Liu, S.; Qiu, Y.; Liu, Y.; Zhang, W.; Dai, Z.; Srivastava, D.; Kumar, A.; Pan, Y.; Liu, J. Recent advances in bimetallic metal—Organic frameworks (BMOFs): Synthesis, applications and challenges. *New J. Chem.* **2022**, *46*, 13818–13837. [CrossRef]
53. Barreda, O.; Bannwart, G.; Yap, G.P.A.; Bloch, E.D. Ligand-Based Phase Control in Porous Molecular Assemblies. *ACS Appl. Mater. Interfaces* **2018**, *10*, 11420–11424. [CrossRef]
54. Smulders, M.M.J.; Jiménez, A.; Nitschke, J.R. Integrative Self-Sorting Synthesis of a Fe8Pt6L24 Cubic Cage. *Angew. Chem. Int. Ed.* **2012**, *51*, 6681–6685. [CrossRef]
55. Teo, J.M.; Coghlan, C.J.; Evans, J.D.; Tsivion, E.; Head-Gordon, M.; Sumby, C.J.; Doonan, C.J. Hetero-Bimetallic Metal-Organic Polyhedra. *Chem. Commun.* **2016**, *52*, 276–279. [CrossRef]

56. Maity, M.; Howlader, P.; Mukherjee, P.S. Coordination-Driven Self-Assembly of Cyclopentadienyl-Capped Heterometallic Zr—Pd Cages. *Cryst. Growth Des.* **2018**, *18*, 6956–6964. [CrossRef]
57. Li, F.; Lindoy, L.F. Metalloligand Strategies for Assembling Heteronuclear Nanocages—Recent Developments. *Aust. J. Chem.* **2019**, *72*, 731–741. [CrossRef]
58. Planes, O.M.; Jansze, S.M.; Scopelliti, R.; Fadaei-Tirani, F.; Severin, K. Two-Step Synthesis of Linear and Bent Dicarboxylic Acid Metalloligands with Lengths of up to 3 Nm. *Inorg. Chem.* **2020**, *59*, 14544–14548. [CrossRef] [PubMed]
59. Hardy, M.; Struch, N.; Topić, F.; Schnakenburg, G.; Rissanen, K.; Lützen, A. Stepwise Construction of Heterobimetallic Cages by an Extended Molecular Library Approach. *Inorg. Chem.* **2018**, *57*, 3507–3515. [CrossRef] [PubMed]
60. Reichel, F.; Clegg, J.K.; Gloe, K.; Gloe, K.; Weigand, J.J.; Reynolds, J.K.; Li, C.-G.; Aldrich-Wright, J.R.; Kepert, C.J.; Lindoy, L.F. Self-Assembly of an Imidazolate-Bridged Fe^{III}/Cu^{II} Heterometallic Cage. *Inorg. Chem.* **2014**, *53*, 688–690. [CrossRef]
61. Lisboa, L.S.; Findlay, J.A.; Wright, L.J.; Hartinger, C.G.; Crowley, J.D. A Reduced-Symmetry Heterobimetallic $[PdPtL_4]^{4+}$ Cage: Assembly, Guest Binding, and Stimulus-Induced Switching. *Angew. Chem. Int. Ed.* **2020**, *59*, 11101–11107. [CrossRef]
62. Carpenter, J.P.; Ronson, T.K.; Rizzuto, F.J.; Héliot, T.; Grice, P.; Nitschke, J.R. Incorporation of a Phosphino(Pyridine) Subcomponent Enables the Formation of Cages with Homobimetallic and Heterobimetallic Vertices. *J. Am. Chem. Soc.* **2022**, *144*, 8467–8473. [CrossRef]
63. Liu, G.; Zeller, M.; Su, K.; Pang, J.; Ju, Z.; Yuan, D.; Hong, M. Controlled Orthogonal Self-Assembly of Heterometal-Decorated Coordination Cages. *Chem. Eur. J.* **2016**, *22*, 17345–17350. [CrossRef]
64. Liu, J.; Wang, Z.; Cheng, P.; Zaworotko, M.J.; Chen, Y.; Zhang, Z. Post-Synthetic Modifications of Metal—Organic Cages. *Nat. Rev. Chem.* **2022**, *6*, 339–356. [CrossRef]
65. Markwell-Heys, A.W.; Roemelt, M.; Slattery, A.D.; Linder-Patton, O.M.; Bloch, W.M. Linking Metal—Organic Cages Pairwise as a Design Approach for Assembling Multivariate Crystalline Materials. *Chem. Sci.* **2021**, *13*, 68–73. [CrossRef]
66. Albalad, J.; Hernández-López, L.; Carné-Sánchez, A.; Maspoch, D. Surface Chemistry of Metal—Organic Polyhedra. *Chem. Commun.* **2022**, *58*, 2443–2454. [CrossRef] [PubMed]
67. Schneider, M.L.; Linder-Patton, O.M.; Bloch, W.M. A Covalent Deprotection Strategy for Assembling Supramolecular Coordination Polymers from Metal-Organic Cages. *Chem. Commun.* **2020**, *56*, 12969–12972. [CrossRef] [PubMed]
68. Schneider, M.L.; Markwell-Heys, A.W.; Linder-Patton, O.M.; Bloch, W.M. Assembly and Covalent Cross-Linking of an Amine-Functionalised Metal-Organic Cage. *Front. Chem.* **2021**, *9*, 696081. [CrossRef]
69. Carné-Sánchez, A.; Craig, G.A.; Larpent, P.; Hirose, T.; Higuchi, M.; Kitagawa, S.; Matsuda, K.; Urayama, K.; Furukawa, S. Self-Assembly of Metal—Organic Polyhedra into Supramolecular Polymers with Intrinsic Microporosity. *Nat. Commun.* **2018**, *9*, 2506. [CrossRef]
70. Yong, M.T.; Linder-Patton, O.M.; Bloch, W.M. Assembly of a Heterometallic Cu(II)-Pd(II) Cage by Post-assembly Metal Insertion. *Inorg. Chem.* **2022**, *61*, 12863–12869. [CrossRef] [PubMed]
71. Pettinari, C.; Pettinari, R. Metal Derivatives of Poly(Pyrazolyl)-Alkanes: II. Bis(Pyrazolyl)Alkanes and Related Systems. *Coord. Chem. Rev.* **2005**, *249*, 663–691. [CrossRef]
72. Bloch, W.M.; Doonan, C.J.; Sumby, C.J. Using Hinged Ligands to Target Structurally Flexible Copper (Ii) MOFs. *CrystEngComm* **2013**, *15*, 9663–9671. [CrossRef]
73. Bloch, W.M.; Doonan, C.J.; Sumby, C.J. Tuning Packing, Structural Flexibility, and Porosity in 2D Metal—Organic Frameworks by Metal Node Choice. *Aust. J. Chem.* **2019**, *72*, 797–804. [CrossRef]
74. Bloch, W.M.; Burgun, A.; Coghlan, C.J.; Lee, R.; Coote, M.L.; Doonan, C.J.; Sumby, C.J. Capturing Snapshots of Post-Synthetic Metallation Chemistry in Metal—Organic Frameworks. *Nat. Chem.* **2014**, *6*, 906–912. [CrossRef]
75. Bloch, W.M.; Babarao, R.; Hill, M.R.; Doonan, C.J.; Sumby, C.J. Post-Synthetic Structural Processing in a Metal—Organic Framework Material as a Mechanism for Exceptional CO_2/N_2 Selectivity. *J. Am. Chem. Soc.* **2013**, *135*, 10441–10448. [CrossRef]
76. Evans, J.D.; Sumby, C.J.; Doonan, C.J. Post-Synthetic Metalation of Metal-Organic Frameworks. *Chem. Soc. Rev.* **2014**, *43*, 5933–5951. [CrossRef]
77. Martín Díaz, A.E.; Lewis, J.E.M. Structural Flexibility in Metal-Organic Cages. *Front. Chem.* **2021**, *9*, 706462. [CrossRef] [PubMed]
78. Ahmadi, M.; Panahi, F.; Bahri-Laleh, N.; Sabzi, M.; Pareras, G.; Falcone, B.N.; Poater, A. pH-Responsive Gelation in Metallo-Supramolecular Polymers Based on the Protic Pyridinedicarboxamide Ligand. *Chem. Mater.* **2022**, *13*, 6155–6169. [CrossRef]
79. De, S.; Mahata, K.; Schmittel, M. Metal-Coordination-Driven Dynamic Heteroleptic Architectures. *Chem. Soc. Rev.* **2010**, *39*, 1555–1575. [CrossRef]
80. Mayer, I. Charge, bond order and valence in the AB initio SCF theory. *Chem. Phys. Lett.* **1983**, *97*, 270–274. [CrossRef]
81. Poater, A.; Gallegos Saliner, A.; Solà, M.; Cavallo, L.; Worth, A.P. Computational Methods to Predict the Reactivity of Nanoparticles Through Structure-Property Relationships. *Expert Opin. Drug Deliv.* **2010**, *7*, 295–305. [CrossRef]
82. Poater, A.; Moradell, S.; Pinilla, E.; Poater, J.; Solà, M.; Martínez, M.A.; Llobet, A. A trinuclear Pt(II) compound with short Pt–Pt–Pt contacts. An analysis of the influence of π–π stacking interactions on the strength and length of the Pt–Pt bond. *Dalton Trans.* **2006**, *9*, 1188–1196. [CrossRef]
83. Asadi, Z.; Sadjadi, S.; Nekoomanesh-Haghighi, M.; Posada-Pérez, S.; Solà, M.; Bahri-Laleh, N.; Poater, A. Lubricant hydrogenation over a functionalized clay-based Pd catalyst: A combined computational and experimental study. *Appl. Organomet. Chem.* **2022**, *36*, e6850. [CrossRef]

84. Bosson, J.; Poater, A.; Cavallo, L.; Nolan, S.P. Mechanism of Racemization of Chiral Alcohols Mediated by 16-Electron Ruthenium Complexes. *J. Am. Chem. Soc.* **2010**, *132*, 13146–13149. [CrossRef]
85. Johnson, E.R.; Keinan, S.; Mori-Sanchez, P.; Contreras-Garcia, J.; Cohen, A.J.; Yang, W.T. Revealing noncovalent interactions. *J. Am. Chem. Soc.* **2010**, *132*, 6498–6506. [CrossRef]
86. Contreras-Garcia, J.; Johnson, E.R.; Keinan, S.; Chaudret, R.; Piquemal, J.P.; Beratan, D.N.; Yang, W.T. NCIPLOT: A program for plotting noncovalent interaction regions. *J. Chem. Theory Comput.* **2011**, *7*, 625–632. [CrossRef]
87. Lattanzi, A.; De Fusco, C.; Russo, A.; Poater, A.; Cavallo, L. Hexafluorobenzene: A powerful solvent for a noncovalent stereoselective organocatalytic Michael addition reaction. *Chem. Commun.* **2012**, *48*, 1650–1652. [CrossRef]
88. Lal, G.; Gelfand, B.S.; Lin, J.-B.; Banerjee, A.; Trudel, S.; Shimizu, G.K.H. Three Sequential Hydrolysis Products of the Ubiq-uitous Cu_{24} Isophthalate Metal—Organic Polyhedra. *Inorg. Chem.* **2019**, *58*, 9874–9881. [CrossRef]
89. Mallick, A.; Garai, B.; Díaz, D.D.; Banerjee, R. Hydrolytic Conversion of a Metal—Organic Polyhedron into a Metal—Organic Framework. *Angew. Chem. Int. Ed.* **2013**, *52*, 13755–13759. [CrossRef]
90. Poater, A.; Vummaleti, S.V.C.; Pump, E.; Cavallo, L. Comparing Ru and Fe-catalyzed olefin metathesis. *Dalton Trans.* **2014**, *43*, 11216–11220. [CrossRef]
91. Luque-Urrutia, J.A.; Solà, M.; Milstein, D.; Poater, A. Mechanism of the Manganese-Pincer Catalyzed Acceptorless Dehydrogenative Coupling of Nitriles and Alcohols. *J. Am. Chem. Soc.* **2019**, *141*, 2398–2403. [CrossRef]
92. Hanifpour, A.; Bahri-Laleh, N.; Nekoomanesh-Haghighi, M.; Poater, A. Group IV diamine bis(phenolate) catalysts for 1-decene oligomerization. *Mol. Catal.* **2020**, *493*, 111047. [CrossRef]
93. Frisch, M.J.; Trucks, G.W.; Schlegel, H.B.; Scuseria, G.E.; Robb, M.A.; Cheeseman, J.R.; Scalmani, G.; Barone, V.; Petersson, G.A.; Nakatsuji, H.; et al. *Gaussian 16, Revision C.01*; Gaussian, Inc.: Wallingford, CT, USA, 2016.
94. Zhao, Y.; Truhlar, D.G. The M06 suite of density functionals for main group thermochemistry, thermochemical kinetics, noncovalent interactions, excited states, and transition elements: Two new functionals and systematic testing of four M06-class functionals and 12 other functionals. *Theor. Chem. Acc.* **2008**, *120*, 215–241.
95. Weigend, F.; Ahlrichs, R. Balanced basis sets of split valence, triple zeta valence and quadruple zeta valence quality for H to Rn: Design and assessment of accuracy. *Phys. Chem. Chem. Phys.* **2005**, *7*, 3297–3305. [CrossRef]
96. Weigend, F. Accurate Coulomb-fitting basis sets for H to Rn. *Phys. Chem. Chem. Phys.* **2006**, *8*, 1057–1065. [CrossRef]
97. Marenich, A.V.; Cramer, C.J.; Truhlar, D.G. Universal solvation model based on solute electron density and on a continuum model of the solvent defined by the bulk dielectric constant and atomic surface tensions. *J. Phys. Chem. B* **2009**, *113*, 6378–6396. [CrossRef]
98. Wang, C.; Shang, J.; Tian, L.; Zhao, H.-W.; Wang, P.; Feng, K.; He, G.-K.; Liu, J.Z.; Zhu, W.; Li, G.-T. Direct identification of HMX via guest-induced fluorescence turn-on of molecular cage. *Chin. Chem. Lett.* **2022**, *32*, 4006–4010. [CrossRef]
99. Lisboa, L.S.; Preston, D.; McAdam, C.J.; Wright, L.J.; Hartinger, C.G.; Crowley, J.D. Heterotrimetallic Double Cavity Cages: Syntheses and Selective Guest Binding. *Angew. Chem. Int. Ed.* **2022**, *61*, e202201700. [CrossRef]

Disclaimer/Publisher's Note: The statements, opinions and data contained in all publications are solely those of the individual author(s) and contributor(s) and not of MDPI and/or the editor(s). MDPI and/or the editor(s) disclaim responsibility for any injury to people or property resulting from any ideas, methods, instructions or products referred to in the content.